Journal of Magnetic Resonance **139,** 126–131 (1999)
Article ID jmre.1999.1760, available online at http://www.idealibrary.com on IDEAL®

The Spin Coherence Relaxation in the Rotating Frame as a Microscopy Parameter for Strongly Coupled Spin Systems

F. De Luca,* E. De Vita,§ G. H. Raza,‡ and C. Casieri†

**Istituto Nazionale di Fisica della Materia, Sezione Roma1, and Dipartimento di Fisica, Unversitá "La Sapienza," I-00185 Roma, Italy; †Istituto Nazionale di Fisica della Materia and Dipartimento di Fisica, Universitá dell'Aquila, I-67100 L'Aquila, Italy; ‡Glaxo Wellcome Medicines Research Center, via A. Fleming 4, I-37135 Verona, Italy; and §Chemistry Department, University of Illinois at Chicago, Chicago, Illinois 60607*

Received December 7, 1998; revised March 17, 1999

The transverse relaxation time in the rotating frame $T_{2\rho}$ is proposed as an effective parameter to get specific contrast in solid state imaging. Several peculiarities make $T_{2\rho}$ an interesting candidate to map dynamics and structure in solids: the effect of the secular spin interaction can be controlled by the experimenter and therefore the relaxation associated with the nonsecular terms, which is particularly sensitive to very slow dynamics, can be observed. In this paper we present preliminary results obtained on polymers and prove the capability of the MARF Imaging, enhanced by a filter based on rotary echo refocusing, to produce images of solids contrasted by $T_{2\rho}$.

INTRODUCTION

In the past few years, *c*oherent *a*veraging-assisted *s*olid *s*tate *i*maging (CASSI) methods (*1, 2*) have been recognised as effective procedures for the NMR approach to microscopy of solid-like materials, even though their potentialities have not been fully exploited.

Notwithstanding their experimental complexity, CASSI methods are able to provide maps of solid samples by means of NMR parameters that can provide information on the microscopic structure and dynamics of solids (*3–5*). The wide availability of localized information makes CASSI methods competitive with respect to well-established higher-resolution microscopies.

Among the NMR parameters utilized for CASSI contrast, the relaxation times in the rotating frame seem particularly promising (*6, 7*). When dealing with relaxation times in the rotating frame we generally refer to $T_{1\rho}$, the spin–lattice relaxation time; only a few papers deal with the transverse relaxation time $T_{2\rho}$ (*8–10*). The reason that, so far, little effort has been devoted to the study of $T_{2\rho}$ is probably the experimental difficulties: In fact, not only is $T_{2\rho}$ sensitive to the same spin dynamics influencing $T_{1\rho}$, but it also presents some features very interesting for both CASSI contrast and relaxometry.

In the weak collision approximation (*11*), the $T_{2\rho}$ zero frequency term depends by a Wigner matrix of the Euler angles expressing the relative orientation of a tilted rotating frame (TRF: $x'y'z'$, where $B_e\hat{z}'$ and B_e is the effective Zeeman magnetic field) with respect to the laboratory frame (LF: xyz, where $B_0\hat{z}$ and B_0 is the main Zeeman magnetic field). The rank of the matrix depends on spin interaction: Hamiltonians that are linear in the spin operator (chemical shift, heteronuclear dipolar, etc.) originate first-rank transformation in spin-space, whereas bilinear interactions (homonuclear dipolar, quadrupolar) transform by a second-rank Wigner matrix (*12*).

For every Hamiltonian there is a particular value of the angle between the two Zeeman axes z and z' that makes the secular part of the Hamiltonians vanish in the TRF; a collapse of the linewidth of solids is observed, and the value of the angle is usually referred as the "magic angle." Our approach to CASSI is founded on this outcome (*13, 14*). So the first consequence of a $T_{2\rho}$-based contrast could be a map of the efficiency with which the secular Hamiltonian is cancelled across the sample or a measure of the distribution of microscopic interactions across the sample. The spatial variation in the effect of the magic angle could be due, for example, to variation of the arrangement of interacting spins across the sample or to the fact that the dominant spin Hamiltonian changes as a consequence of structural inhomogeneities (*15*).

A detailed analysis of $T_{2\rho}$ dispersion shows that the range of spin dynamics to which $T_{2\rho}$ is sensitive extends to motion slower than that detectable via $T_{1\rho}$, T_{2e}, and T_{1D}. It is known that in the ordinary weak collision theory the direct correlation between $T_{1\rho}$ and the spin dynamics characterized by a rate τ_c^{-1} applies only in a range outside $\gamma B_e \tau_c \gg 1$, where γ is the gyromagnetic ratio (*16, 17*). An interesting calculation developed by Atsarkin and colleagues (*18, 19*) shows that the explicit dependence of $T_{2\rho}$ on the magic angle from molecular motion extends to the limit

$$\left(\frac{B_e}{\gamma B_L^2}\right) > \tau_c \gg \frac{1}{\gamma B_e},$$

where B_L is the average local field. Since the ratio B_e/B_L can be set to a rather high value, $T_{2\rho}$ results can correlate down to ultraslow molecular motion, that is, motion characterized by a

1090-7807/99 $30.00

rate $\tau_c^{-1} \approx 10^2\ \mathrm{sec}^{-1}$. Such features could make $T_{2\rho}$ an effective parameter for detection and analysis of very slow molecular motion in solids.

In this paper we present a first CASSI method that allows $T_{2\rho}$-contrasted NMR images to be obtained and that is easily extended to $T_{2\rho}$ measures for relaxometric purposes. Preliminary monodimensional $T_{2\rho}$ maps of some solid polymer samples are presented.

THEORY

The transformation from LF to TRF for a generic random spin Hamiltonian can be expressed as

$$\sum_{m=-l}^{l} (-1)^m A_{lm} F_{l-m}(t) \Rightarrow \sum_{mm'} (-1)^m e^{-im'\alpha} d^{(l)}_{m'm}(\theta) e^{-im\beta} A_{lm} F_{l-m}(t), \qquad [1]$$

where the scalar product of the irreducible l-rank spherical tensors A_{lm} and $F_{lm'}$ dependent on spin and random coordinates, is projected in the TRF by means of the reduced Wigner matrix $d_{mm'}$ and rotation operators of angles

$$\alpha = \omega t;\ \theta = tg^{-1}\left(\frac{\gamma B_1}{\omega_0 - \omega}\right);$$

$$\beta = \omega_e t = \gamma B_e t = \gamma\left[\left(\frac{\omega_0 - \omega}{\gamma}\right)^2 + B_1^2\right]^{1/2} t.$$

Here $\omega \cong \omega_0 = \gamma B_0$ is the frequency of the oscillating magnetic field $2B_1 \cos \omega t$.

The weak collision approach to relaxation gives, for the bilinear spin Hamiltonian (*8*),

$$\frac{1}{T_{2\rho}} \propto \sum_{mm'} (d^{(2)}_{mm'}(\theta))^2 (m' + 2)(3 - m') J(m\omega_0 + m'\omega_e), \qquad [2]$$

where J is the reduced spectral density of the correlation function $\langle F_{lm}(0) F^*_{lm}(t)\rangle$, and for linear spin Hamiltonians the equation

$$\frac{1}{T_{2\rho}} \propto \sum_{mm'} (d^{(1)}_{mm'}(\theta))^2 (m' + 1)(2 - m') J(m\omega_0 + m'\omega_e). \qquad [3]$$

For example, by supposing exponential correlation of the random tensor, for a system of dipolar interacting spins Eq. [2] gives

$$\frac{1}{T_{2\rho}} \propto \tau_c\left([d^{(2)}_{00}(\theta)]^2 + \frac{[d^{(2)}_{01}(\theta)]^2 + [d^{(2)}_{0-1}(\theta)]^2}{1 + \omega_e^2\tau_c^2} + \frac{[d^{(2)}_{02}(\theta)]^2 + [d^{(2)}_{0-2}(\theta)]^2}{1 + 4\omega_e^2\tau_c^2}\right). \qquad [4]$$

As in the LF, the dispersion of $T_{2\rho}$ and $T_{1\rho}$ also differ in practice only by the $J(0)$ term (*20*). Such a term can be modified by changing the relative orientation between the LF and TRF, that is, modifying the ratio between the resonant frequency offset and the radio frequency field intensity. From Eqs. [2]–[4] it is evident that a map of a solid contrasted by $T_{2\rho}$ would be able to show the distribution of the reduced Wigner matrix across the sample.

To extend the sensitivity of Eqs. [2]–[4] to $\omega_e\tau_c \gg 1$, a perturbation order greater than 2 should be used to evaluate $T_{2\rho}$ in the weak collision limit $B_e \gg B_L$ and $T_{2\rho} \gg \tau_c$. The approach of Atsarkin and Khazanovich (*19*) shows that the direct correlation of $T_{2\rho}$ extends to molecular motion as slow as $\omega_e\tau_c \gg 1$ by a calculation that reduces the nonsecular terms of the dipolar Hamiltonian to an effective secular Hamiltonian in the TRF. Such a procedure begins from the simple consideration that the TRF linewidth in a rigid solid does not vanish completely even at $\theta = \theta_M$ because of terms contained in the nonsecular Hamiltonian. Therefore the effective secular Hamiltonian H^0_E for a pair of dipolar coupled $\frac{1}{2}$ spins in the isotropic regime (*21*) is given by

$$H^0_E \cong \langle H^0_{ES}\rangle + H^0_{ER} \equiv \langle H^0_{ES}\rangle - \frac{\omega_L^2}{2\omega_e} I_z + \frac{3}{8\omega_e}\sum_{i\neq j} B_{ij}^2 I_{iz}, \qquad [5]$$

where $\langle H^0_{ES}\rangle$ is the average over the lattice variables that produces a small frequency shift from ω_e, and H^0_{ER} contributes to relaxation because $B_{ij}(t) = \gamma^2\hbar^2\mu_0/8\pi r^3(1 - 3\cos^2\vartheta_{ij}(t))$, where $\vartheta_{ij}(t)$ is the angle of the dipolar axis with respect to $\hat{z}$, is in general time-dependent.

By introducing a local frequency in the TRF defined as $\omega^2_{EL} = \mathrm{Tr}[\langle (H^0_{RS})^2\rangle]/\mathrm{Tr}[I_z^2] = 2\omega_L^4/7\omega_e^2$, it is possible to show that the relaxation in the range $\tau_c \gg 1/\omega_e$ results from the Hamiltonian H^0_{ER} (in the second perturbative order this limit makes the nonsecular terms of Eq. [1] negligible), while in the range $\tau_c \ll 1/\omega_{EL}$ the Hamiltonian H^0_{ER} is small enough to be neglected and the relaxation is mainly driven by the usual nonsecular terms. Considering the whole range of correlation from $\tau_c \gg 1/\omega_e$ to $\tau_c \leq 1/\omega_e$, one gets for the transverse relaxation time dispersion the equation (*19*)

$$\frac{1}{T_{2\rho}} = \omega^2_{EL}\tau_c + \frac{\omega_L^2\tau_c}{3}\left[\frac{5}{1 + \omega_e^2\tau_c^2} + \frac{1}{1 + 4\omega_e^2\tau_c^2}\right], \qquad [6]$$

where a simple Lorentzian shape has been supposed for the

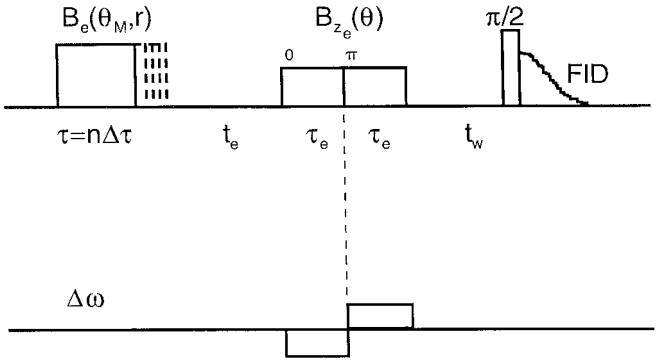

FIG. 1. The MARF imaging sequence with the rotary echo filter. The first part of the sequence is composed of the spatial encoding period, in which the effective field is set to θ_M and made spatially dependent by an effective gradient that is not reported in the figure. After a time $t_e \gg T_2$, a rotary echo is generated by two pulses, each τ_e long, with a phase difference of π: Such a phase difference coupled to an opportune inversion of the resonance off set $\Delta\omega$ is able to invert the effective field or to change the angle of the effective field from θ to $\theta + \pi$. The echo pulses back the TRF magnetization on the z axis so that $t_W \to 0$ and the signal observed after the $\pi/2$ read pulse is those at the end of the spatial encoding period modulated by the $T_{2\rho}$ relaxation during $2\tau_e$. All the inhomogeneity effects due to the radiofrequency field and on the main Zeeman field are therefore eliminated from the signal because of the echo mechanism.

spectral density. The ultraslow-motion term originating from H^0_{ER} produces an ascending branch in the $1/T_{2\rho}$ dispersion curve that causes a minimum at $\tau_c \approx 1/\omega_L$. Equation [6] has been confirmed by numerical simulation and experimental results (*22*).

Our approach to $T_{2\rho}$-contrasted CASSI is based on the pulse sequence reported in Fig. 1. The sequence is based on MARF (magic angle in the rotating frame) imaging (*2*), which uses the magic angle values associated with the reduced Wigner matrices to make the secular term of the spin interaction Hamiltonian vanish (*14*). The MARF spatial constraint is obtained by imposing an effective gradient $G_e = \sqrt{G_0^2 + G_1^2}$ (where G_0 and G_1 are, respectively, dc and radiofrequency gradients) aligned along the effective field to make the coherent averaging effect independent by spatial coordinates. The result is a liquid-like space encoded line, with $\omega_e(r) = \gamma B_e + \gamma G_e r$. The time evolution of the magnetization in the TRF is reconstructed stepwise, by use of the first available point of the LF-FID acquired (*7*).

In the sequence of Fig. 1 the spatially independent $T_{2\rho}$ filter is turned on after a time $t_e \gg T_2$ from the end of the spatial encoding pulse to avoid influence of the spatial encoding period on the $T_{2\rho}$ filter. The filter is made of two radiofrequency pulses of same length τ_e phase shifted by π. Intensity and resonant offset of the two filter pulses are set in such a way as to select the appropriate values of θ and B_e; obviously the values of θ and/or of B_e may be different from the ones used during the spatial encoding pulse. The π phase shift associated to the inversion of the resonant offset produces a rotation by an angle π of the B_e axis (the second echo pulse rotates the TRF of an angle $\theta + \pi$ with respect to the z axis), thus allowing a TRF echo refocusing (*10, 23*). The interval $2\tau_e$ determines the duration of $T_{2\rho}$ evolution that can be varied, as well as the B_e intensity, to make the image contrast dependent by the spatial setting of the reduced Wigner matrix or, via Eq. [6], by dynamics.

In the high-field approximation, provided that $B_e(r) \gg B_L$, the propagator

$$P_{LG} = \exp[-i\gamma B_e(\theta_M)\hat{I}_{z'}n\Delta\tau - i\gamma(\mathbf{G}_e(\theta_M)\cdot\mathbf{r})\hat{I}_{z'}n\Delta\tau - iH^*(\theta_M)n\Delta\tau] \quad [7]$$

describes the TRF line-narrowing space-encoded signal at the end of the space encoding period of the sequence of Fig. 1 for a total pulse duration of $n\Delta\tau$. Imposing that $\gamma\|(\mathbf{G}_e(\theta_M)\cdot\Delta\mathbf{r})\hat{I}_{z'}\| \gg \|H^*(\theta_M)\|$, where $H^*(\theta_M)$ is the spin interaction residual at the magic angle and Δr the spatial resolution, under the condition $N\Delta\tau \gg T_{2\rho}(\theta_M, r)$, where $N\Delta\tau$ is the maximum duration of the space encoding pulse, the density operator at the end of t_e is given by (*7*)

$$\rho(n\Delta\tau + t_e) \propto [\cos^2\theta_M + \sin^2\theta_M\cos(\omega_e(r)n\Delta\tau)]I_Z. \quad [8]$$

The TRF echo pulses introduce the operators $\exp[\pm i\omega_{z_e}\tau_e I_{z_e}]$, which describe the clockwise and counterclockwise rotation at frequency ω_{z_e} around the echo effective field B_{z_e} forming an angle θ with the z axis. Assuming a time-independent dipolar Hamiltonian, at the end of the $2\tau_e$ period the propagator $\exp[-iH^0(\theta)2\tau_e]$, where H^0 is the truncated dipolar Hamiltonian, describes the action of the filter (the shift associated with $\langle H^0_{ES}\rangle$ is negligible when $\theta \neq \theta_M$; on the other hand when $\theta = \theta_M$ the propagator has the form $\exp[-i\langle H^0_{ES}\rangle 2\tau_e]$) and the space-dependent linewidth would only be dependent by the local setting of the reduced Wigner matrix. Since in general the spin interaction is time dependent, when the secular spin interaction term is not efficient as a coherence loss mechanism, as in the case of $\theta \approx \theta_M$ or conditions similar to those that yield Eq. [6], the $T_{2\rho}$ relaxation becomes "visible" and the TRF signal after the $\pi/2$ pulse is given by (because at the echo maximum the magnetization is back to the z axis and $t_W \approx 0$; otherwise, the condition $t_W \gg T_2$ should be fulfilled)

$$m_+(r, \tau_e) = m_{0S}(r)\exp\left[-\frac{2\tau_e}{T_{2\rho}(\theta, \omega_{z_e})}\right], \quad [9]$$

supposing, for the sake of simplicity, a simple exponential form for the decay of the TRF signal, and where

$$m_{0S}(r) = \frac{\gamma^2\hbar^2N(r)I(I+1)}{3kT_S(r)}B_0 \quad [10]$$

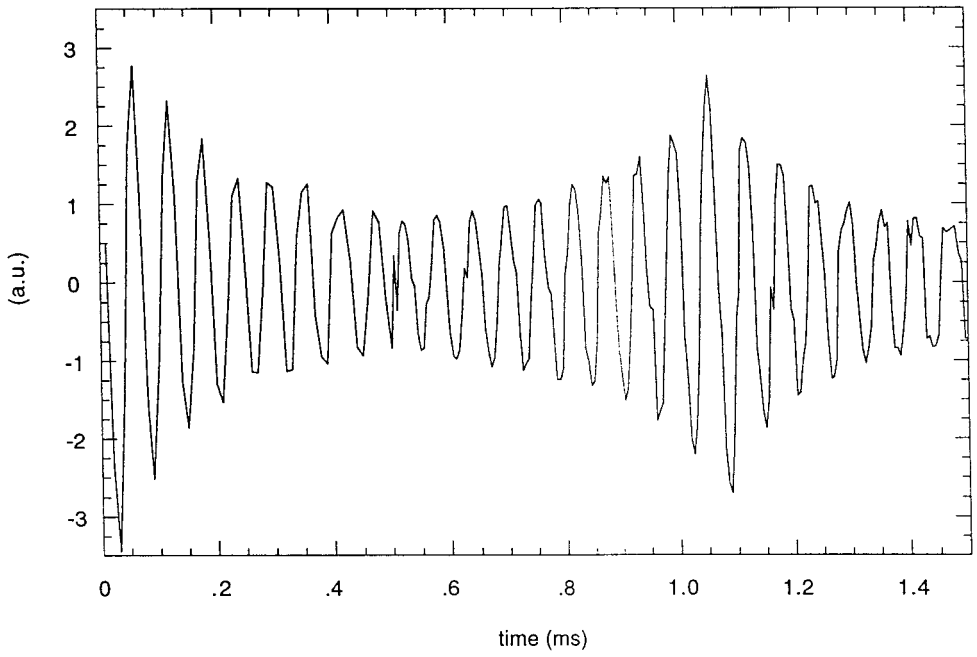

FIG. 2. The TRF echo of Vulkollan obtained by the sequence of Fig. 1 without the spatial encoding part. In this case the first echo pulse length has been stepped from 0 to 0.5 ms to get the TRF-FID, and therefore, maintaining the length of the first pulse fixed to 0.5 ms, the second echo pulse has been stepped from 0 to about 1 ms: when the second pulse reaches a length of about 0.5 ms, there is the rotary echo refocusing. Of course when the length of the second echo pulse is different from that of the first pulse, the condition $t_W \gg T_2$ must be fulfilled because in the TRF transversal plane, magnetisation components survive that have components on the LF transversal plane that relax via T_2.

is the local r-positioned equilibrium magnetization at $T_S(r)$, the local (equilibrium) spin temperature, given by

$$T_S(r) = \frac{T_L}{\cos^2\theta_M + \sin^2\theta_M \cos[\omega_e(r) n\Delta\tau]}, \qquad [11]$$

where T_L is the lattice temperature. $N(r)$ is the number of spins per unit volume at position r. Equation [11] also assumes that T_1 is much longer than the duration of the whole sequence of Fig. 1.

The discrete Fourier transform of the detected signal from the whole sample, whose extension along r is L, can be written as

$$S(m\Delta\omega) = \frac{\hbar^2\gamma^2 I(I+1)}{3kT_L} B_0 \sin^2\theta_M \int_L dr N(r) e^{-2\tau_e/T_{2\rho}(\theta,\omega_e)} \times \sum_n \cos[\omega_e(r) n\Delta\tau] e^{-im\Delta\omega n\Delta\tau} + C(0), \qquad [12]$$

where $C(0)$ is a zero-frequency term originated by the cosine term of Eq. [8] and m is the index of the frequency sampling.

EXPERIMENTAL RESULTS AND COMMENTS

As first experimental result we report a TRF echo obtained by the sequence of Fig. 1 without the spatial encoding part. The TRF echo of a sample of Vulkollan (polyurethane elastomer, about 3 kHz half-intensity linewidth) is reported in Fig. 2. The first part of the figure was obtained recording the intensities of the signal after a single echo pulse ranging from 0 to 500 μs, while in the second part (500 to 1400) the first pulse of 500 μs was followed by the phase shifted pulse with duration increased step by step from 0 to 900 μs. The effective frequency was about 15 kHz, $\theta = 90°$, and $\omega_0 \cong 30$ MHz. In Fig. 2, both the TRF-FID and the echo are fully observable, the echo being refocused at $2\tau_e = 1$ ms. By exploring the echo amplitude for different τ_e's the $T_{2\rho}$ relaxation can be measured owing to the field inhomogeneity (mostly due to B_1). In Fig. 3 the TRF transverse relaxation at $\omega_0 \cong 30$ MHz of Vulkollan, adamantane (about 20 kHz half-intensity linewidth), Plexiglas (about 50 kHz half-intensity linewidth), and Delrin (polyacetal, about 25 kHz half-intensity linewidth) are reported for $\gamma B_{z_e} \approx 60$ kHz and $\theta = 90°$. The data reported in Fig. 3 show an oscillation superimposed on the decay (that, up to now, we have not been able to explain either as systematic experimental error or as a physical effect and makes the fitting uncertain). The echo maximum envelope of Fig. 3 can roughly be fitted by Eq. [9], which gives $T_{2\rho} \approx 50$ μs for Plexiglas, $T_{2\rho} \approx 80$ μs for Delrin, and $T_{2\rho} \approx 85$ μs for adamantane, while that of

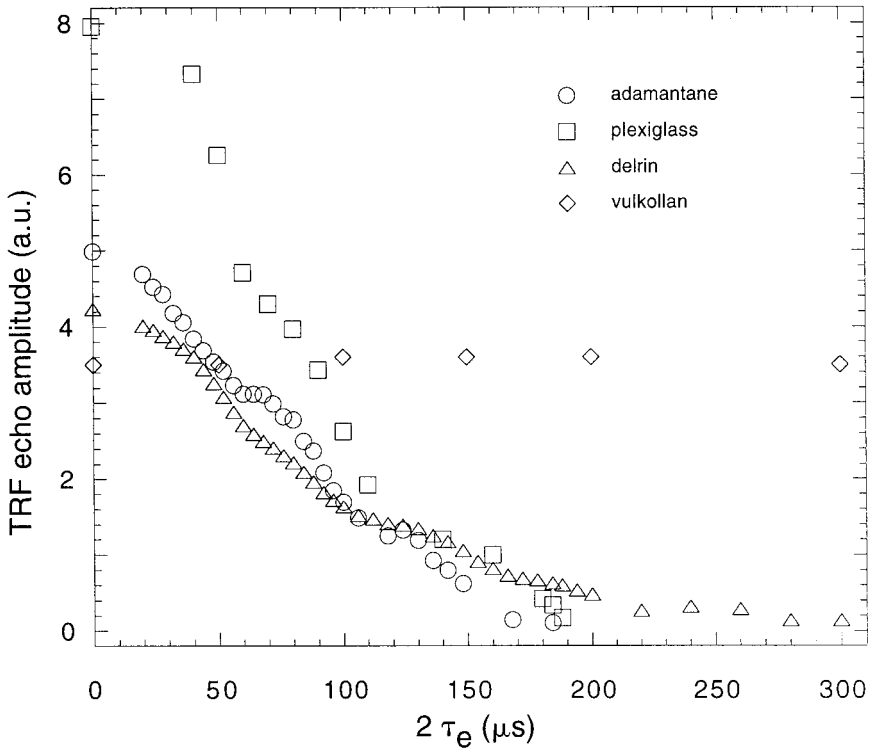

FIG. 3. In this figure the $T_{2\rho}$ relaxations of some solids are reported. Also in this case the sequence used is that of Fig. 1 without the spatial encoding part. All the experimental points, each corresponding to the TRF echo maximum, show an oscillating behavior that, up to now, we have not been able to explain. The data can roughly be fitted by an exponential function.

Vulkollan can only be estimated to be >20 ms. Such results, although affected by large errors that probably mask a biexponential relaxation, are indicative of the activity of the nonsecular terms of the dipolar Hamiltonian. In fact, the dipolar interaction at our Zeeman field is presumably the dominant interaction in these solid samples, and the reduced Wigner matrix effect at $\theta = 90°$ should just halve the linewidth with respect to that produced by the full secular term.

In all these experiments, as well as in those reported below, we kept $\theta = 90°$ since we had problems realizing the switching of the resonance offset, sketched in the sequence of Fig. 1, in a time $t_s \ll 2\pi\omega_{z_e}^{-1}$, owing to the eddy current's effect on the poles of our electromagnet (our RF source has no phase-lock).

In Fig. 4 a projection series acquired with the full sequence of Fig. 1 is shown. The sample, sketched at the top of the figure, was composed of pieces of Delrin and Plexiglas separated by a Teflon spacer. All the profiles have been obtained by setting the spatial encoding part of the sequence in the typical MARF condition, namely, $\omega_e \approx 78$ kHz, $\theta = \theta_M$, $t_e = 3$ ms, $\Delta\tau = 5$ μs, $N = 120$, and an effective gradient $G_e = 27$ mT/m. Each signal has been averaged three times with a repetition time (recycle delay) of 2 s. Each spatial profile corresponds to the TRF echo maximum with different τ_e's and the fixed values $\theta = 90°$ and $\omega_{z_e} \approx 60$ kHz.

From the decay of the intensity of the Delrin and Plexiglas peaks at different τ_e's in Fig. 4, it is possible to determine their $T_{2\rho}$ values, which are about 60 μs for Delrin and about 47 μs for Plexiglas, in good agreement with the values obtained by the direct measurements reported in Fig. 3.

Another set of spatial profiles contrasted by $T_{2\rho}$ is reported in Fig. 5. Here the sample is composed of adamantane and

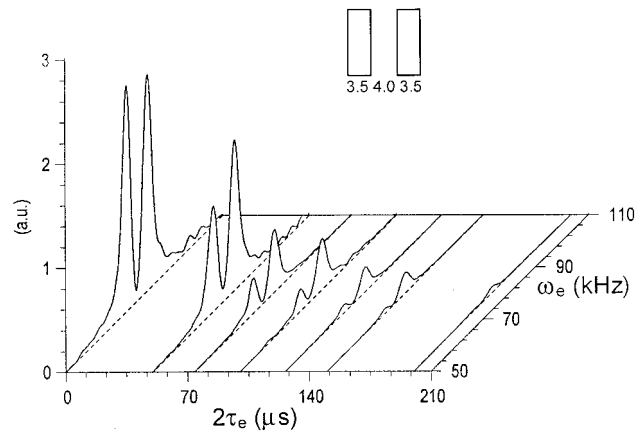

FIG. 4. $T_{2\rho}$-contrasted spatial profiles of the sample at the top of the figure, where the dimensions are in millimeters. The sample consists of one piece of Plexiglas (lower frequency peak) and one of Delrin. The profiles correspond to the echo maximum and have been obtained by the full sequence of Fig. 1. The effective gradient is directed along the transverse direction of the sample. The decay rate of the signals match reasonably well with the ones obtained in Fig. 3.

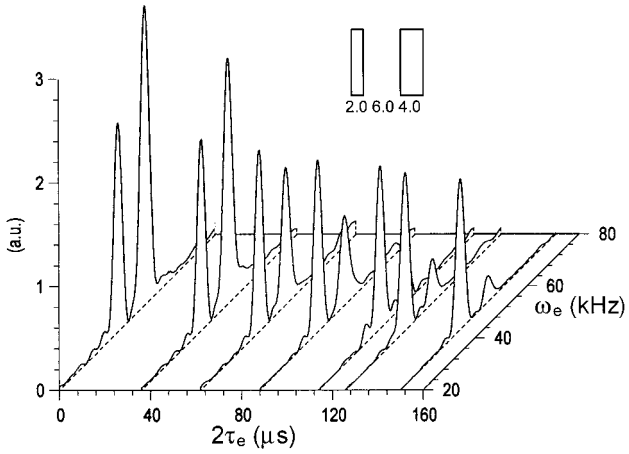

FIG. 5. $T_{2\rho}$-contrasted spatial profiles of the sample sketched at the top of the figure (dimensions in mm). The sample consists of a piece of Vulkollan (lower frequency peak) and one of adamantane. As before, the profiles correspond to the echo maximum and have been obtained by the full sequence of Fig. 1. The decay rate of the signals match reasonably well with the ones obtained in Fig. 3, also in the presence of a strong difference between the $T_{2\rho}$ of the materials involved in the sample.

Vulkollan, which approximates the comparison between a rigid solid and one with liquid-like behavior. In this case the effective gradient was $G_e = 28$ mT/m and $\omega_e \approx 50$ kHz, while the other parameters are the same as those used for the previous sample. The profiles of Fig. 4 not only show the capability of our method to get the same spatial resolution independently of the sample's linewidth, but also demonstrate that even for very different relaxation times, as in presence of liquid-like dynamics, the $T_{2\rho}$ constitutes a good contrast parameter. Also from the profiles of Fig. 5 it is possible to measure the $T_{2\rho}$, and the same results reported in Fig. 3 are obtained: for the adamantane, about 75 μs; while for Vulkollan, as in Fig. 3, it is only possible to give a lower value because is too long with respect to our experimentally accessible $2\tau_e$ range.

We reported the first use of the transverse relaxation in the TRF as a parameter for CASSI. The pulse sequence we utilize is based on the MARF approach to CASSI, which, including $T_{2\rho}$ and the Hartmann–Hahn filters (*24*), has explored up to now most of the NMR parameters as CASSI contrast parameters. The results we obtained with the $T_{2\rho}$ echo filter show that $T_{2\rho}$ spatial mapping and $T_{2\rho}$ relaxometry are practicable and also desirable, $T_{2\rho}$ being richer than $T_{1\rho}$ in information concerning very slow molecular mobility. The measurement of $T_{2\rho}$ for relaxometric purposes is as simple as that of $T_{1\rho}$ at $\theta = \pi/2$ (of course, all the terms of $T_{1\rho}$ dispersion depend on θ). For relaxometric purposes, in fact, the sequence of Fig. 1 reduces to the echo and $\pi/2$ pulses only with $t_W = 0$. It is in practice a sort of upsetting of the sequence used for $T_{1\rho}$: In the $T_{2\rho}$ measurement the magnetization is rotated in the LF transverse plane after $T_{2\rho}$ relaxation; the $T_{1\rho}$ measure, in contrast, provides the $\pi/2$ rotation before $T_{1\rho}$ relaxation. As for $T_{1\rho}$, by sampling the initial LF-FID amplitude, which supplies the echo maximum amplitude, the $T_{2\rho}$ measurement can be performed.

The main goal of this paper was to show that a solid-state map contrasted by $T_{2\rho}$ is possible and that the effect of the $T_{2\rho}$ relaxation gives the same results with and without spatial encoding. The informational content of $T_{2\rho}$ concerning dynamics and structure of spin systems has been outlined in the introduction and in the preceding section and, although it could be analyzed in more detail, some indications of the potentiality of $T_{2\rho}$ should be evident.

REFERENCES

1. See, for example, *Solid State NMR,* **6**(4), 275–401 (1996). Special Issue on Magnetic Resonance Imaging of Materials.
2. F. De Luca, G. H. Raza, A. Gargaro, and B. Maraviglia, *J. Magn. Reson.* **126,** 159 (1997).
3. R. Kimmich, "NMR Tomography, Diffusometry, Relaxometry," Springer-Verlag, Berlin (1997).
4. S. Matsui, A. Uraoka, and T. Inouye, *J. Magn. Reson. A* **120,** 11 (1996).
5. A. Guthausen, G. Zimmer, P. Blümler, and B. Blümich, *J. Magn. Reson.* **130,** 1 (1998).
6. B. Blümich, P. Blümer, E. Günter, J. Jansen, G. Schauss, and H. W. Spiess, "Magnetic Resonance Microscopy," VCH, Weinheim (1992), pp. 167–185.
7. F. De Luca, A. Gargaro, B. Maraviglia, G. H. Raza, and C. Casieri, *Magn. Reson. Imag.* **16**(4), 435 (1998).
8. J. S. Blicharski, *Acta Physica Polonica* **A41,** 223 (1972).
9. D. Wolf, "Spin-Temperature and Nuclear-Spin Relaxation in Matter," Clarendon Press, Oxford (1979).
10. H. Kessemeir, Won-Kyu Rhim, *Phys. Rev. B* **5,** 761 (1972).
11. D. C. Ailion, *Adv. Magn. Reson.* **5,** 1977 (1971).
12. N. Lugeri, F. De Luca, B. C. De Simone, and B. Maraviglia, "CXXIII Corso, Scuola Internazionale di Fisica "Enrico Fermi," North-Holland, Amsterdam (1993), pp. 449–471.
13. F. De Luca, N. Lugeri, B. C. De Simone, and B. Maraviglia, *Solid State Commun.* **82,** 151 (1992).
14. M. Lee, W. I. Goldburg, *Phys. Rev.* **140**(4A), 1261 (1965).
15. K. Schmidt-Rohr and H. W. Spiess, "Multidimensional Solid-State NMR and Polymers," Academic Press, San Diego (1994).
16. M. Mehering, "Principles of High Resolution NMR in Solids," Springer-Verlag, Berlin (1983).
17. D. C. Look and I. J. Lowe, *J. Chem. Phys.* **44**(8), 2995 (1966).
18. V. A. Atsarkin, A. E. Mefed, and M. I. Rodak, *Sov. Phys. Solid State* **21,** 1537 (1979).
19. V. A. Atsarkin and T. N. Khazanovich, *Sov. Phys. JETP* **60**(1), 162 (1984).
20. C. P. Slichter, "Principles of Magnetic Resonance," Springer-Verlag, Berlin (1990).
21. U. Haeberlen and J. S. Waugh, *Phys. Rev.* **185,** 420 (1969).
22. A. F. Mefed, V. A. Atsarkin, *Phys. Status Solidi A* **93,** 21 (1986).
23. I. Solomon, *Phys. Rev. Lett.* **2,** 301 (1959).
24. C. Casieri, F. De Luca, B. Maraviglia, and F. Santoro, *in* "Proceed. Joint 29th AMPERE-13th ISMAR International Conference," Berlin (1998), pp. 565–566.